

# Experimental and Theoretical Study of Aerodynamic Characteristics of Some Lifting Bodies at Angles of Attack From $-10^\circ$ to $53^\circ$ at Mach Numbers From 2.30 to 4.62

---

*M. Leroy Spearman and Abel O. Torres*  
*Langley Research Center • Hampton, Virginia*



## Summary

An experimental and theoretical design study has been made of a generic family of lifting body configurations. The configurations all had a  $75^\circ$  swept delta planform with a rounded nose, but they had different upper and lower surface camber shapes. The camber shapes varied in thickness and in the location of the maximum thickness. The study consisted of models with a flat bottom and upper surface camber variations, models with a flat top and lower surface camber variations, and models with variations in both upper and lower surface camber. The experimental results were obtained in the Langley Unitary Plan Wind Tunnel at Mach numbers from 2.30 to 4.62 for angles of attack from  $-10^\circ$  to  $53^\circ$  and included both longitudinal and lateral-directional aerodynamic characteristics. The theoretical results were obtained through the use of the Aerodynamic Preliminary Analysis System II.

The results show that changes in the camber design cause distinct changes in the aerodynamic characteristics that should be considered in the selection of a lifting-body shape. In general, the flat-bottom designs with upper surface camber provided greater drag for retardation at high angles of attack, but they were considerably out of trim longitudinally for the chosen moment reference center. The flat-top designs with lower surface camber, on the other hand, provided less drag at high angles of attack but could be more easily trimmed longitudinally.

The generally good agreement between the theoretical and experimental results indicates that the calculative techniques used herein should be a valuable aid in the design process of lifting bodies in the supersonic speed range.

## Introduction

Lifting bodies are of interest for possible use as space transportation vehicles because they have the volume required for significant payloads and the aerodynamic capability to negotiate the transition from high angles of attack to lower angles of attack (for cruise flight) and thus safely reenter the atmosphere and perform conventional horizontal landings. The purpose of the present paper is to discuss the effects of camber variations on the aerodynamic characteristics of some generic lifting-body designs in the transition region from high to low angles of attack at supersonic speeds and to compare the theoretical results with the experimental results. All experimental data presented herein were selected from reference 1 and are included in this paper for the convenience of the reader. An abbreviated version of this paper was also presented in a conference (ref. 2).

## Symbols

$b$	planform span
$C_D$	drag coefficient, Drag/ $qS$
$C_L$	lift coefficient, Lift/ $qS$
$C_l$	rolling-moment coefficient, Rolling moment/ $qSb$
$C_{l\beta}$	effective dihedral parameter (rolling moment due to sideslip)
$C_m$	pitching-moment coefficient, Pitching moment/ $qSl$
$C_n$	yawing-moment coefficient, Yawing moment/ $qSb$
$C_{n\beta}$	directional stability parameter (yawing moment due to sideslip)
$C_Y$	side-force coefficient, Side force/ $qS$
$C_{Y\beta}$	side-force parameter (side force due to sideslip)
$c$	chord
c.g.	center-of-gravity location, percent body length
$L/D$	lift-drag ratio
$l$	body length
$M$	Mach number
$q$	free-stream dynamic pressure
$S$	planform area
$t$	thickness
$V$	volume
$X$	longitudinal distance from model nose, in.
$Z$	vertical distance from model centerline, in.
$\alpha$	angle of attack, deg
$\beta$	angle of sideslip, deg
Abbreviations:	
max	maximum
OSU	Ohio State University
rad.	radius

Model designations:

- L        body lower surface
- LF       body with flat lower surface (flat bottom)
- U        body upper surface
- UF       body with flat upper surface (flat top)

## Models and Tests

The geometry of the test models is shown in figure 1. The models all had a  $75^\circ$  delta planform with a rounded nose and, with the exception of the flat-top and flat-bottom bodies, had elliptical cross sections with varied upper and lower surface camber shapes. The coordinates of the camber shapes at the model centerline are given in table I, and the volumes of the test models are given in table II. A balance housing was attached to the models in such a way that the balance moment reference center was vertically offset from the horizontal reference plane. For the flat-bottom models, the balance housing was imbedded in the upper surface (fig. 1(a)). The flat-bottom models were inverted to provide the flat-top models, which then had the balance housing imbedded in the lower surface. For models with both upper and lower surface camber, the balance housing was imbedded in the upper surface (figs. 1(b) 1(d)). The model designations are given in chart A.

Chart A

Designation	Surface	Maximum $t/c$ location, percent $c$	$t/c$
UF	Upper	Flat	0
LF	Lower	Flat	0
U3010	Upper	30	10
U3020	Upper	30	20
U5020	Upper	50	20
L3010	Lower	30	10
L3020	Lower	30	20
L5020	Lower	50	20
L7010	Lower	70	10
L7020	Lower	70	20

A six-component strain gauge balance was mounted in the balance housing with the balance moment reference center located longitudinally at 53 percent of the body length and displaced vertically from the horizontal reference plane by 4 percent of the body length. Tests were made in the Langley Unitary Plan Wind Tunnel at Mach numbers of 2.30, 2.96, 3.95, and 4.62 for angles of attack from  $-10^\circ$

to  $53^\circ$  at angles of sideslip of  $0^\circ$  and  $3^\circ$  (ref. 1). Only selected data from reference 1 are repeated in this paper (primarily for  $M = 4.62$  and 2.30). The test Reynolds number was  $2 \times 10^6$  per foot. Gross drag values are presented with no corrections applied for base or balance chamber drag. The angles of attack and sideslip have been corrected for sting and balance deflections and for tunnel flow angularity.

## Accuracy

The estimated accuracies, based on instrument calibration and data repeatability, are given in chart B.

Chart B

$C_L$	0.0020
$C_D$	0.0020
$C_m$	0.0040
$C_l$	0.0015
$C_n$	0.0010
$C_Y$	0.0020
$M$	0.050
$\alpha$ , deg	0.10
$\beta$ , deg	0.10

## Discussion

### Experimental Results

**Comparison of flat-top and flat-bottom designs.** A comparison of the longitudinal characteristics at  $M = 4.62$  for L5020 (flat top) and U5020 (flat bottom) is shown in figure 2. In this comparison the cambered surface had  $t/c = 0.20$  located at  $0.50c$  with the result that the volumes were equal. At high angles of attack (representative of a reentry attitude), the flat-bottom design produces significantly high lift and drag but also displays large negative values of pitching moment that require trimming. The flat-top design produces somewhat lower values of lift and drag at the higher angles of attack but displays positive values of pitching moment that improve trim characteristics. The results indicate that at an angle of attack of  $0^\circ$  the flat-bottom design has negative lift and a negative pitching moment, whereas the flat-top design has positive lift and a positive pitching moment. This effect is probably caused by the impact pressure on the forebody. The initial values of pitching moment result in trim characteristics that are adverse for the flat-bottom design and favorable for the flat-top design throughout the angle-of-attack

range. Hence, the differences in  $L/D$  shown in the lower cruising angle-of-attack range would be likely to change when trimmed; the flat-top design would show some improvement and the flat-bottom design would show some impairment.

The lateral-directional results for these flat-bottom and flat-top designs are presented in figure 3. The results show the directional instability that must be overcome is generally greater with the flat top (cambered lower surface) than with the flat bottom (cambered upper surface). Because the side force is greater for the flat-top design, it is apparent that the lateral center of pressure is farther forward for the cambered lower surface than for the cambered upper surface. The vertical location of the lateral center of pressure also affects the rolling moment because the effective dihedral parameter at lower angles of attack is positive (unfavorable) with the cambered upper surface and negative (favorable) with the cambered lower surface. The test models had no directional stability surfaces, and the addition of such surfaces would change the directional stability as well as the effective dihedral.

**Lower surface camber variations with the flat top.** The longitudinal characteristics at  $M = 4.62$  are presented in figure 4 for the flat-top design with variations in the lower surface camber. The camber shapes are labeled L3010, L3020, and L5020 and include a thickness change at a constant chord station and a chord station change for a constant thickness. These results indicate that the longitudinal aerodynamic characteristics are sensitive to the shape of the lower surface camber. The thinner shape (L3010), which has a higher lift-curve slope and a higher maximum  $L/D$ , has the least volume. A positive increment in pitching moment at an angle of attack of  $0^\circ$  provides a self-trimming characteristic for each of the designs. Increasing the thickness to  $0.20c$  results in a decrease in the lift-curve slope and in the maximum value of  $L/D$ , but a positive shift occurs in the pitching moment that increases the self-trimming capability. The results of the test of L5020 indicate that shifting the maximum thickness point aft changes the lift and drag ratio. However, the most significant change is in the pitching moment, which provides the highest trim angle of attack of the three shapes. Even though the volumes are about the same for L3020 and L5020, the L5020 design provides a higher maximum value of  $L/D$  and better self-trimming characteristics.

The lateral-directional results for these designs (fig. 5) show an increase in the side force, which

should be expected as the thickness is increased. The attendant increase in directional instability is greatest for L3020, the design with the most forward maximum thickness location. The effective dihedral is favorable for all three designs; however, it is reduced by the increase in lower surface thickness because of the increased side force below the roll axis.

**Lower surface camber variations with upper surface U3010.** The longitudinal characteristics at  $M = 4.62$  are presented in figure 6 for the U3010 upper surface with three lower surface shapes, L3020, L7020, and L7010. For the lower surface thickness of  $0.20c$ , a rearward shift in the maximum thickness location from 30 to 70 percent  $c$  (L3020 to L7020) results in little change in volume (table II). However, this shift results in a substantial increase in the high angle-of-attack trim point, an increase in drag at high angles of attack (representative of the reentry attitude), and an increase in  $L/D$  at lower angles of attack (representative of the cruise attitude). When the lower surface thickness at the 70-percent-chord location (L7020 to L7010) is reduced and the volume decreases, the high angle-of-attack trim point decreases but the  $L/D$  in the lower angle-of-attack cruise regime increases.

The lateral-directional characteristics (fig. 7) indicate the greatest directional instability when the maximum thickness is the most forward (L3020). When the lower surface maximum thickness moves rearward (L3020 to L7020), the lateral center of pressure shifts rearward and the directional instability is reduced. Decreasing the thickness (L7010) results in a further reduction in the instability because of a decrease in the side force. The rolling moment due to sideslip is positive for the 20-percent-thick lower surface camber shapes, presumably because the lateral center of pressure is below the roll axis. Decreasing the lower surface thickness to 10 percent causes the center of pressure to move upward and the rolling moment due to sideslip to shift negatively.

**Upper surface camber variations with lower surface L3020.** The longitudinal characteristics at  $M = 4.62$  are presented in figure 8 for the L3020 lower surface with the two upper surface shapes UF and U3010. The effects of these upper surface changes were relatively small. A comparison of the cambered upper surface with the flat upper surface shows increased volume in the upper surface but indicates a decrease in  $L/D$  in the lower angle-of-attack cruise regime.

The lateral-directional characteristics for these designs (fig. 9) indicates that changing from the flat upper surface (UF) to the cambered upper surface

(U3010) moves the effective lateral center of pressure forward and downward so that the directional instability is increased and the rolling moment due to sideslip becomes positive. It should be remembered that for this comparison the balance roll axis is below the model reference plane for the flat top and above the reference plane for the cambered upper surface.

**Upper surface camber variations with lower surface L7010.** The longitudinal characteristics at  $M = 4.62$  are presented in figure 10 for the L7010 lower surface with the three upper surface shapes U3010, U3020, and U5020. These upper surface changes had little effect on the longitudinal aerodynamic characteristics except for the increase in  $L/D$  in the lower angle-of-attack cruise regime for the thinner U3010 camber. However, this shape has an attendant volume decrease compared with the other two upper surface shapes shown. Little difference in the longitudinal characteristics exists between the U3020 and U5020 shapes, and although the camber shapes are different, the volumes are about the same.

The lateral-directional characteristics for these designs are shown in figure 11. Little difference occurs in the rolling-moment parameter as the upper surface camber changes, thus indicating that this parameter is primarily influenced by the lower surface. The side force increases as the thickness increases. The lateral center of pressure is apparently farthest forward for the U3020 shape because this shape has the greatest directional instability.

**Sensitivity to the center-of-gravity location.** The test results presented herein are referenced to an arbitrary moment center or center of gravity (c.g.) located at 53 percent of the body length. Because the longitudinal stability level is dependent on the moment center location, the effect of moderate changes in the c.g. location on the longitudinal stability and trim characteristics was examined, and examples are shown in figure 12 for the U3010/L7020 and UF/L3010 designs. The results for the U3010/L7020 design with a test moment reference point of 53 percent of the body length indicate a high self-trimmed angle of attack that is desirable for reentry but an unstable variation of pitching moment at lower angles of attack. Figure 12 shows that positive longitudinal stability can be achieved over the entire test angle-of-attack range with a relocation of the c.g. from 53 to 46 percent of the body length; however, the trim angle of attack would be lowered.

The results for the UF/L3010 with a moment reference point of 53 percent of the body length indi-

cate positive longitudinal stability over the entire test angle-of-attack range even though the self-trimmed angle of attack is relatively low. A substantially higher trim angle of attack can be obtained with a relocation of the c.g. from 53 to 67 percent of the body length, but longitudinal instability occurs at angles of attack below about  $25^\circ$ .

**Some effects of Mach number.** The effects of Mach number on the longitudinal stability for the UF/L5020 and U3010/L7020 designs for a c.g. at 53 percent of the body length are presented in figure 13. The low-angle-of-attack instability that occurs at  $M = 4.62$  gradually becomes stable at  $M = 2.30$ . Thus, the high trim angles of attack that are desirable for retardation can be maintained and the configurations automatically become stable at lower cruise angles of attack as the Mach number decreases. In addition, both designs have positive values of pitching moment at an angle of attack of  $0^\circ$ , which improves trimming.

**Volumetric efficiency.** The variations of the maximum values of  $L/D$  with volume for each of the test models is presented in figure 14 for  $M = 2.30$  and 4.62. The expected trend of decreasing  $L/D$  with increasing volume is apparent but some camber shapes did not follow the trend. Note that some variations in  $L/D$  occur for constant volume and that some levels of  $L/D$  are maintained even with substantial increases in volume. Attempts to optimize the shape for the maximum  $L/D$  must also consider characteristics such as the longitudinal trim and the lateral-directional stability.

## Theoretical Results

Calculations were made using the Aerodynamic Preliminary Analysis System II and the Hypersonic Arbitrary-Body Aerodynamic Computer Program. (See refs. 3-5.) The methodology used is illustrated in figure 15. In the impact regions of the main body, the Dahlem-Buck empirical method was used from the nose back to the maximum-thickness location, and the modified Newtonian method was used aft of that point. For the shadow regions of the main body, the Prandtl-Meyer expansion from free stream was used. For the balance housing element, the tangent wedge method was used in the impact region and the Ohio State University (OSU) blunt-body empirical method was used in the shadow region. The reference enthalpy method was selected for the viscous analysis with turbulent flow. When the calculations were carried out in either the laminar or transitional modes, the results were the same.

Computer-generated drawings of some of the designs are shown in figure 16. A comparison of the theoretical and experimental results for the U3010/L7010 design is presented in figure 17 for  $M = 4.62$ . The agreement is quite good, especially for the nonlinear variations in lift and pitching moment with angle of attack. A comparison of the same design at a Mach number of 2.30 (fig. 18) shows slightly greater differences in the theoretical and experimental values, but the nonlinear variations are still predicted reasonably well. It is significant that the change in longitudinal stability with Mach number is predicted. This agreement is partly due to the existence of a single shock (bow shock) on these configurations. The boundary layer was well behaved over the entire surface because of the favorable pressure gradient (no separation). The base pressure contribution to drag was insignificant because of the small base area.

A comparison of the results at  $M = 4.62$  for the flat-bottom and flat-top designs with the 5020 camber shapes is shown in figure 19 (flat bottom) and figure 20 (flat top), and the comparison is very good. The accurate prediction of both the shift in pitching moment at an angle of attack of  $0^\circ$  and the nonlinear variations of lift and pitching moment with angle of attack are of particular significance. The lateral-directional characteristics were also calculated for the UF/L5020 design, and the results (fig. 20(b)) are quite good.

From these comparisons the calculation techniques used herein appear to be reasonably valid for the concepts of the lifting body considered, and these techniques should be useful tools in the design process.

## Conclusions

The purpose of this paper has been to present some results that might be useful in the design of lifting-body configurations for possible use as space transportation vehicles. Such lifting bodies are of interest for possible use as space transportation vehicles because they have the volume required for significant payloads and the aerodynamic capability to negotiate the transition from high angles of attack to lower angles of attack (for cruise flight) and thus safely reenter the atmosphere and perform conventional horizontal landings. The concepts that were investigated included variations in camber distribution for both the upper and lower surfaces of a  $75^\circ$  swept delta planform. Experimental results from ex-

tensive wind-tunnel tests have been presented and are compared with some calculated results. Some concluding observations are presented as follows:

1. Flat-bottom concepts with upper surface camber provided greater drag for retardation at high angles of attack, but they would be difficult to trim longitudinally.
2. Flat-top concepts with lower surface camber provided less drag for retardation at high angles of attack but could be more easily trimmed longitudinally.
3. The maximum values of lift-to-drag ( $L/D$ ) ratio generally decreased with increasing volume although some combinations of camber provided an increase in volume with no loss in  $L/D$ .
4. The generally good agreement between theoretical and experimental results indicates that the calculation techniques used should be a valuable aid in the design process of lifting-body vehicles in the supersonic speed range.

NASA Langley Research Center  
Hampton, VA 23681-0001  
December 14, 1993

## References

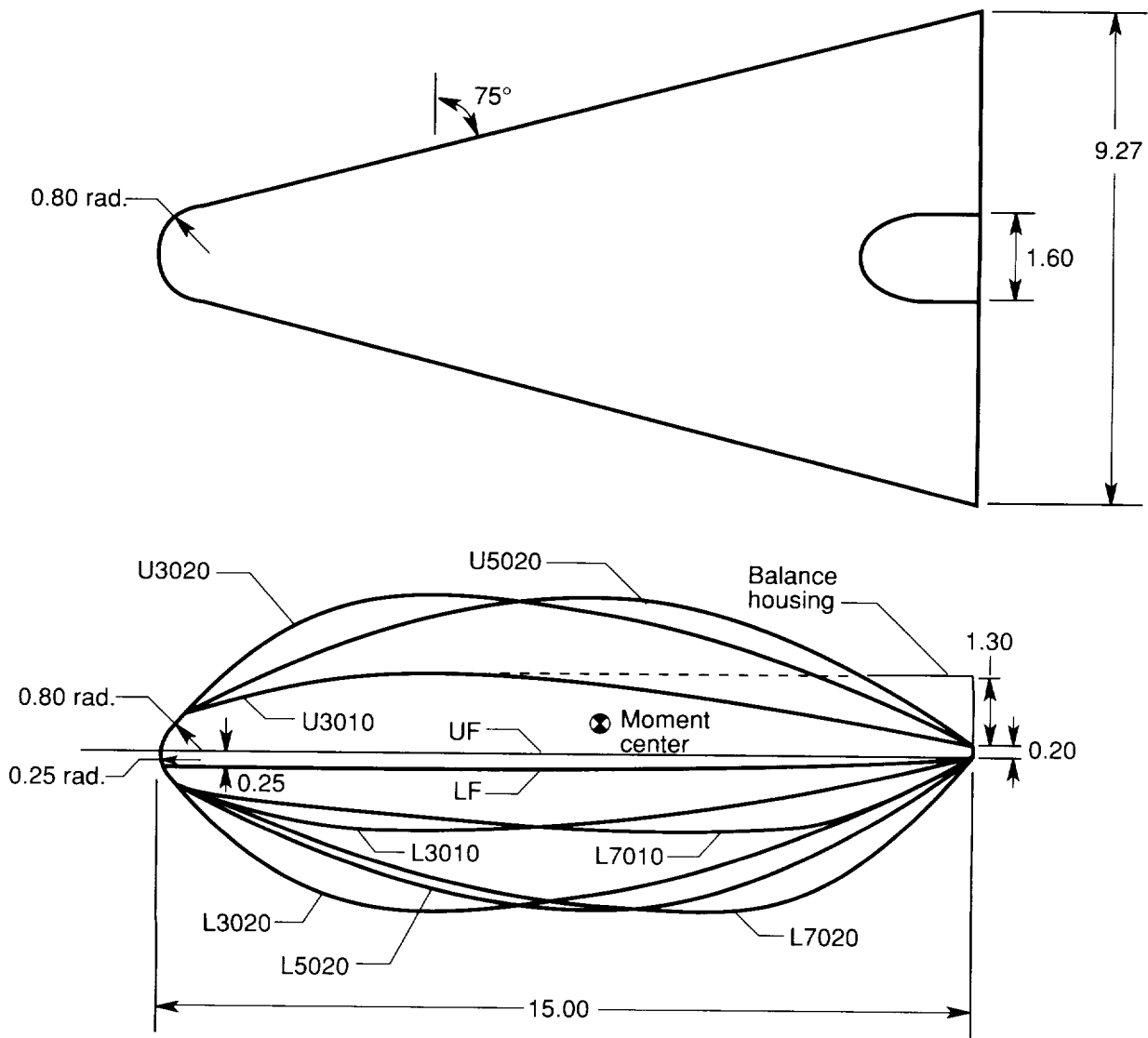
1. Jernell, Lloyd S.; and Fournier, Roger H.: *Effects of Body Camber on Aerodynamic Characteristics of a Lifting Entry Vehicle Model at Mach Numbers From 2.30 to 4.62*. NASA TM X-1217, 1966.
2. Spearman, M. L.; and Torres, Abel O.: An Aerodynamic Design Study of a Series of Lifting Bodies at Angles of Attack From  $-10$  to  $53$  Degrees at Mach Numbers From 2.30 to 4.62. AIAA, Aerospace Design Conference, Paper 8, Feb. 3-6, 1992.
3. Bonner, E.; Clever, W.; and Dum, K.: *Aerodynamic Preliminary Analysis System II. Part I Theory*. NASA CR-182076, 1991.
4. Sova, G.; and Divan, P.: *Aerodynamic Preliminary Analysis System II. Part II User's Manual*. NASA CR-182077, 1991.
5. Gentry, Arvel E.; and Smyth, Douglas N.: *Hyper-sonic Arbitrary-Body Aerodynamic Computer Program (Mark III Version)*. Rep. DAC 61552 (Air Force Contract Nos. F33615 67 C 1008 and F33615 67 C 1602). McDonnell Douglas Corp., Apr. 1968. *Volume I User's Manual*. (Available from DTIC as AD 851 811.) *Volume II Program Formulation and Listings*. (Available from DTIC as AD 851 812.)

Table I. Body Coordinates at Centerline

X, in.	Vertical distance from model centerline (Z), in., for design						
	U3010	U3020	U5020	L3010	L3020	L7010	L7020
1.5	1.04	1.88	1.32	1.04	1.80	0.87	1.17
3.0	1.38	2.72	2.01	1.35	2.70	1.05	1.77
4.5	1.50	3.00	2.54	1.50	3.00	1.20	2.25
6.0	1.47	2.94	2.87	1.47	2.96	1.34	2.61
7.5	1.38	2.76	3.00	1.35	2.75	1.43	2.87
9.0	1.22	2.48	2.90	1.19	2.46	1.49	2.99
10.5	1.04	2.06	2.55	.95	2.04	1.50	3.00
12.0	.77	1.50	1.97	.66	1.47	1.28	2.60
13.5	.47	.87	1.17	.35	.80	.78	1.62
15.0	.20	.20	.20	0	0	0	0

Table II. Volumes of Test Models

Model	V, in <sup>3</sup>
U3010/LF (UF/L3010)	67.42
U3020/LF (UF/L3020)	121.57
U5020/LF (UF/L5020)	121.88
U3010/L7010	132.26
U3020/L7010	186.41
U5020/L7010	186.72
U3010/L3010	128.82
U3010/L3020	188.99
U3010/L7020	190.47



(a) Overlay of several camber shapes.

Figure 1. Model geometry. Dimensions are given in inches unless otherwise noted.



U3010/LF (UF/L3010)

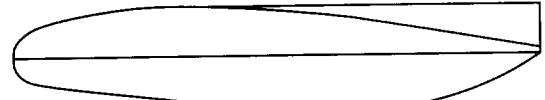


U3020/LF (UF/L3020)

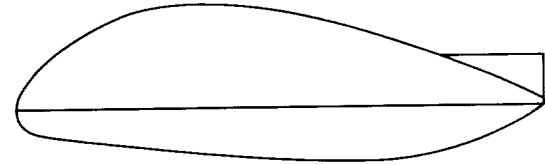


U5020/LF (UF/L5020)

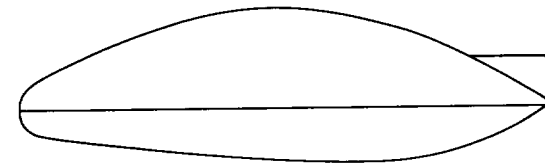
(b) Flat-bottom and flat-top models.



U3010/L7010

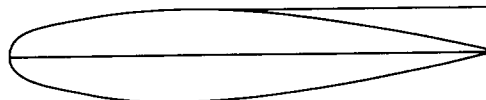


U3020/L7010



U5020/L7010

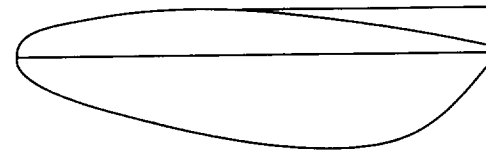
(c) Models with lower surface L7010.



U3010/L3010



U3010/L3020



U3010/L7020

(d) Models with upper surface U3010.

Figure 1. Concluded.

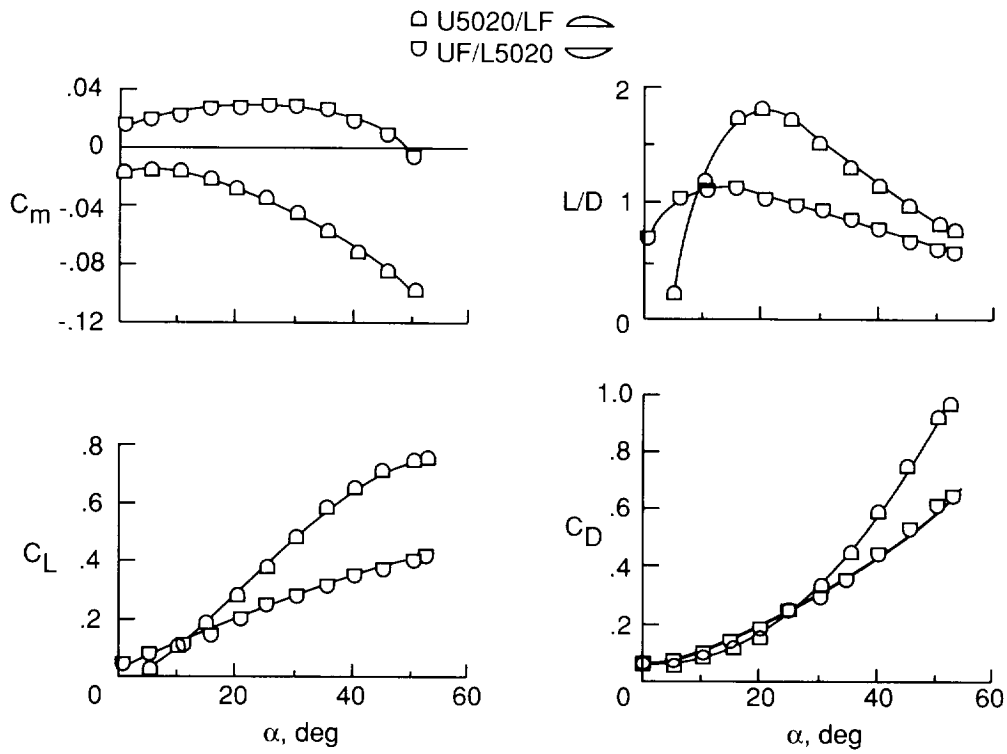


Figure 2. Longitudinal characteristics at  $M = 4.62$  of U5020/LF (flat bottom) and UF/L5020 (flat top).

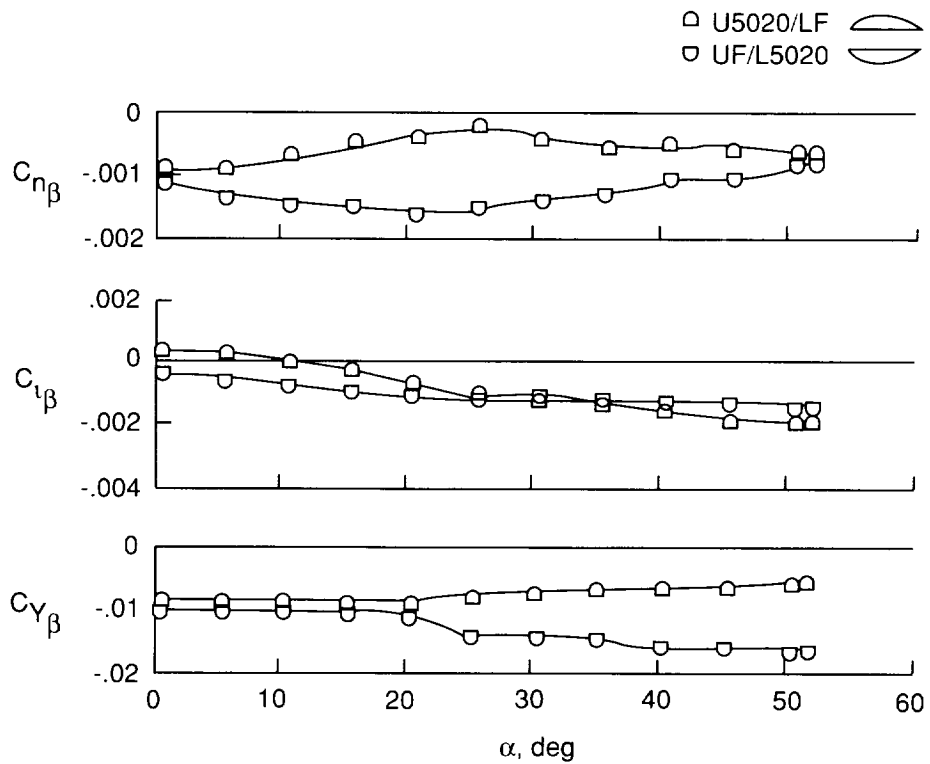


Figure 3. Lateral-directional characteristics at  $M = 4.62$  of U5020/LF (flat bottom) and UF/L5020 (flat top).

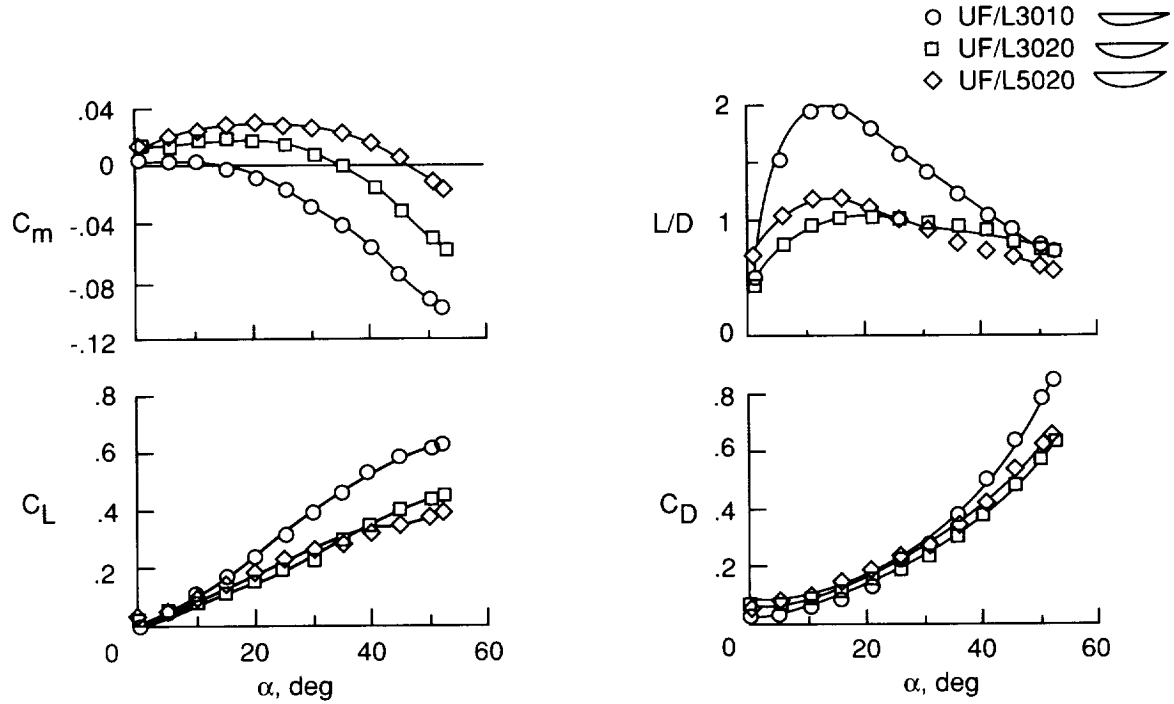


Figure 4. Longitudinal characteristics at  $M = 4.62$  of flat-top design with variations in lower surface camber.

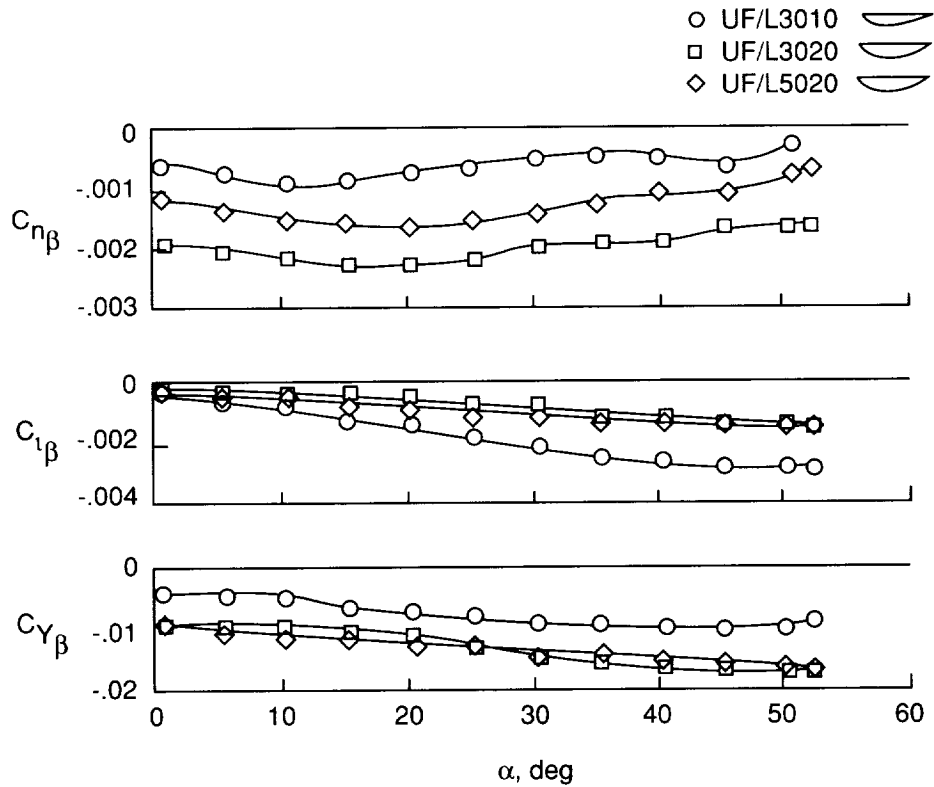


Figure 5. Lateral-directional characteristics at  $M = 4.62$  of flat-top design with variations in lower surface camber.

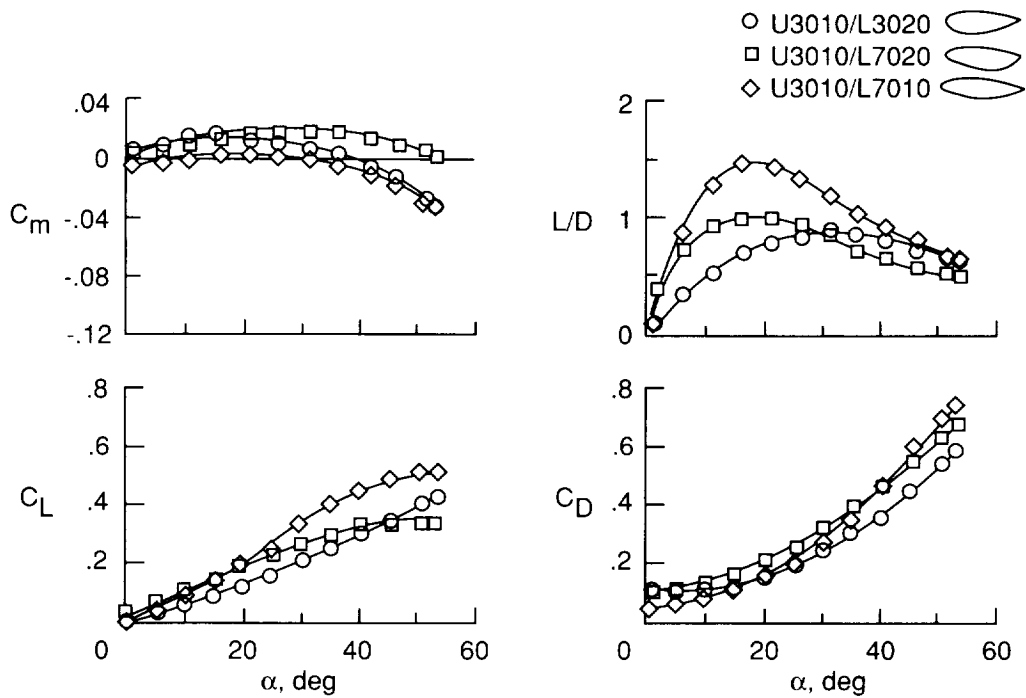


Figure 6. Longitudinal characteristics at  $M = 4.62$  of U3010 with variations in lower surface camber.

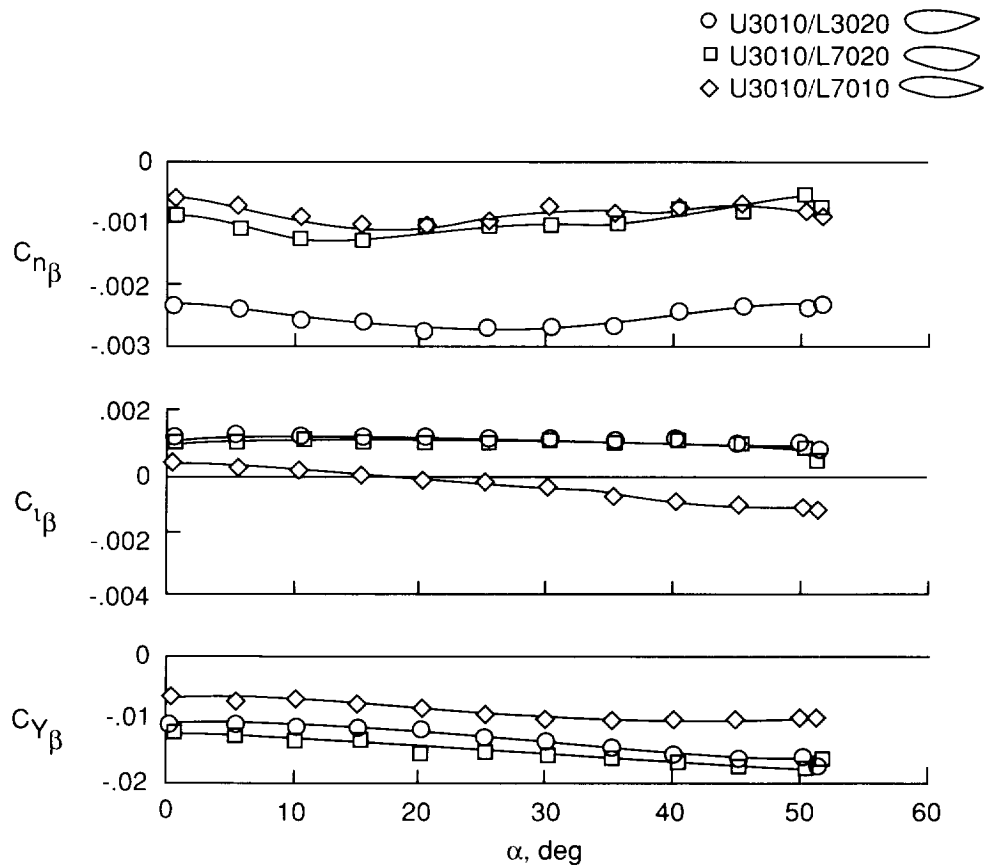


Figure 7. Lateral-directional characteristics at  $M = 4.62$  of U3010 with variations in lower surface camber.

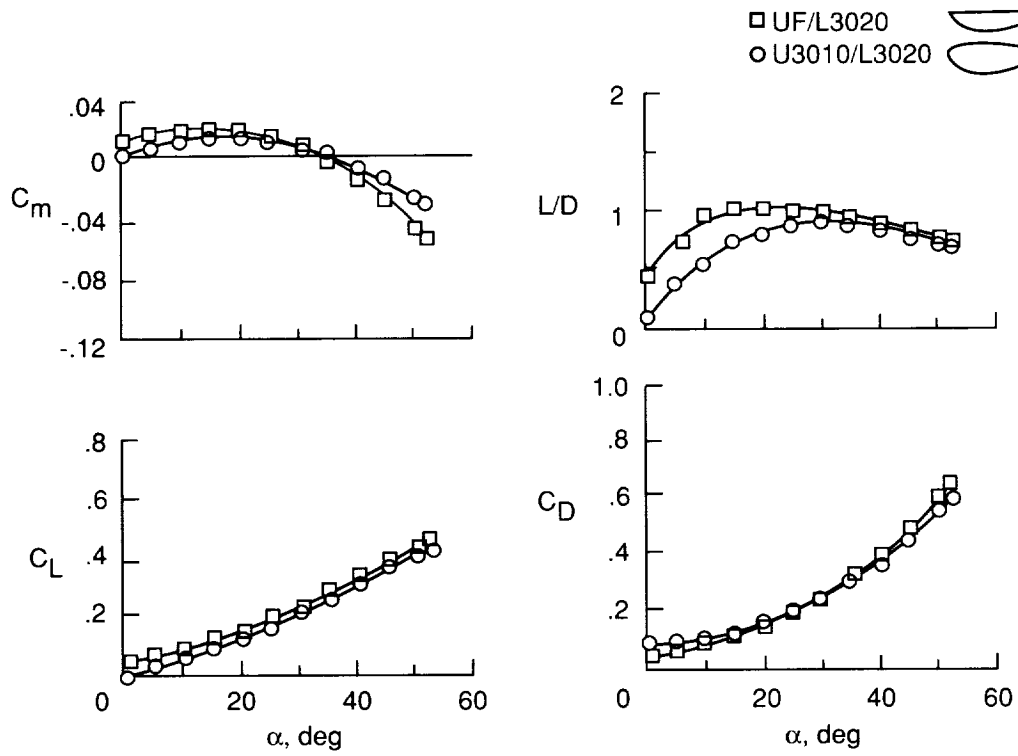


Figure 8. Longitudinal characteristics at  $M = 4.62$  of L3020 with variations in upper surface camber.

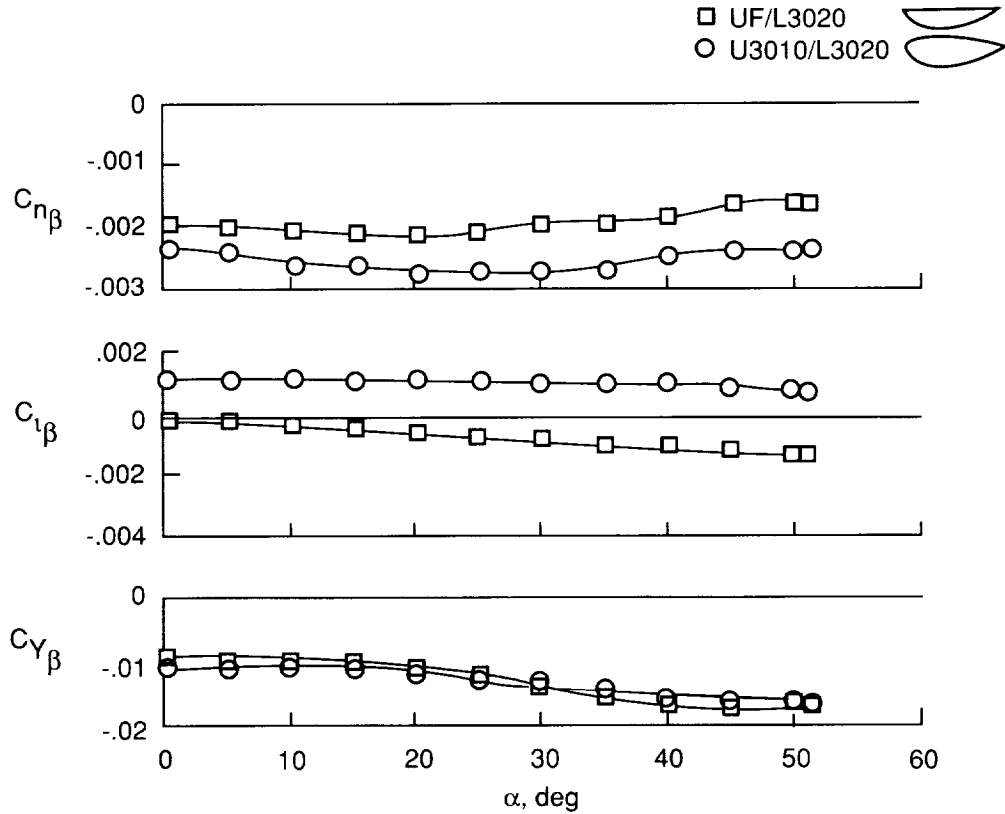


Figure 9. Lateral-directional characteristics at  $M = 4.62$  of L3020 with variations in upper surface camber.

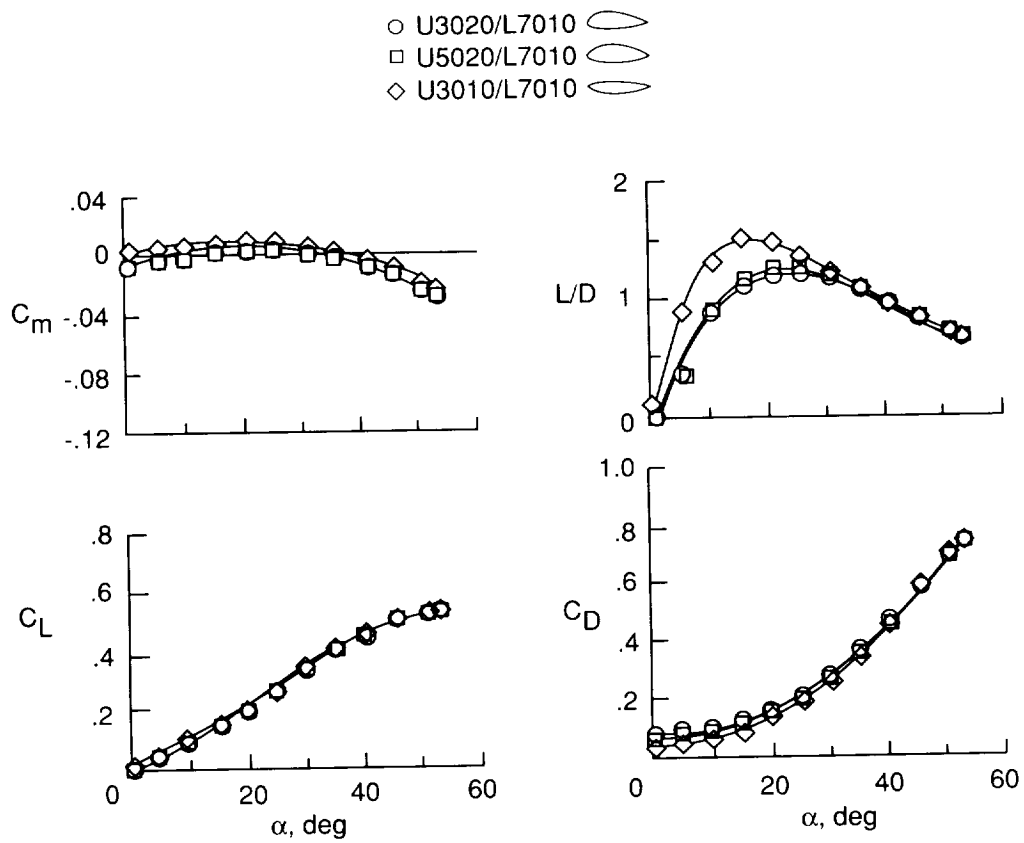


Figure 10. Longitudinal characteristics at  $M = 4.62$  of L7010 with variations in upper surface camber.

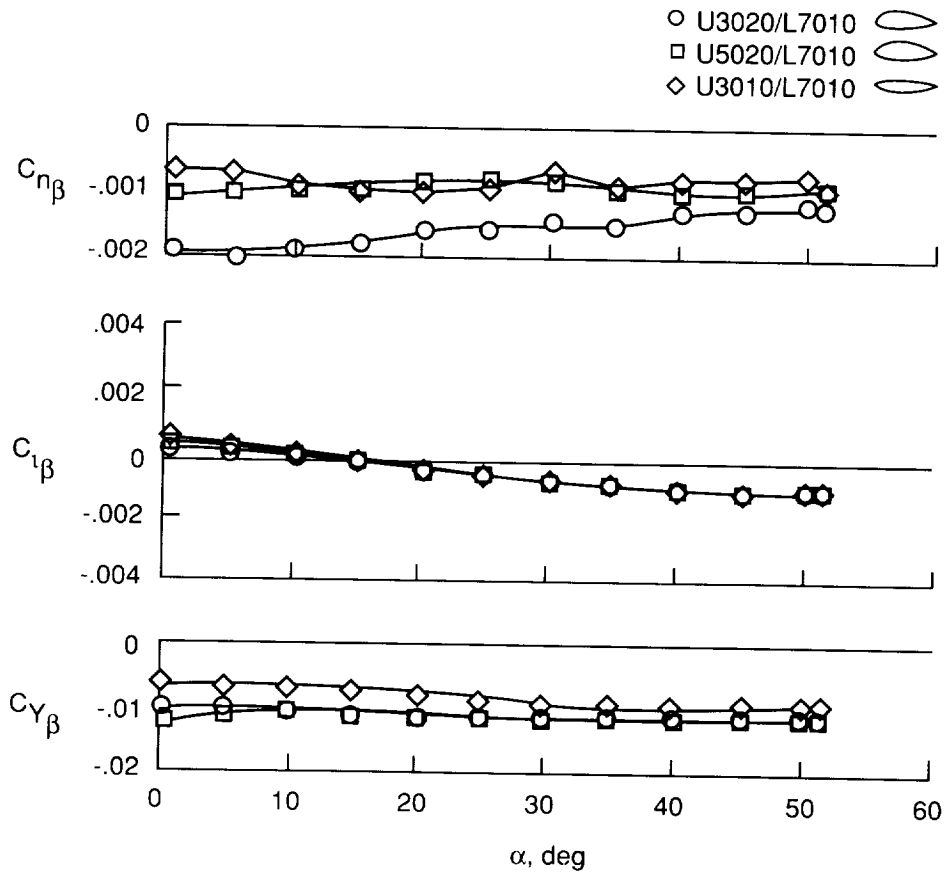


Figure 11. Lateral-directional characteristics at  $M = 4.62$  of L7010 with variations in upper surface camber.

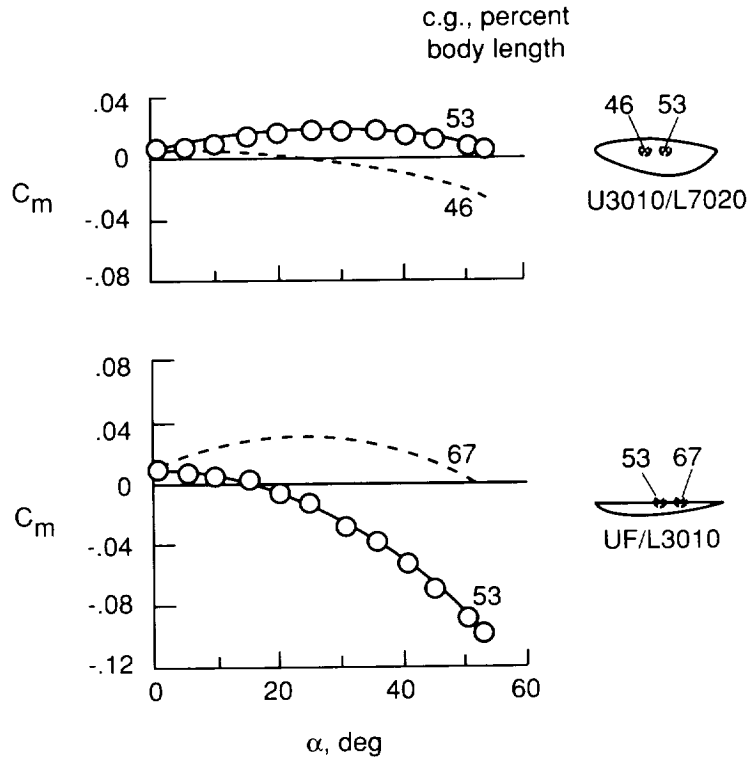


Figure 12. Effect of center-of-gravity location on longitudinal characteristics at  $M = 4.62$ .

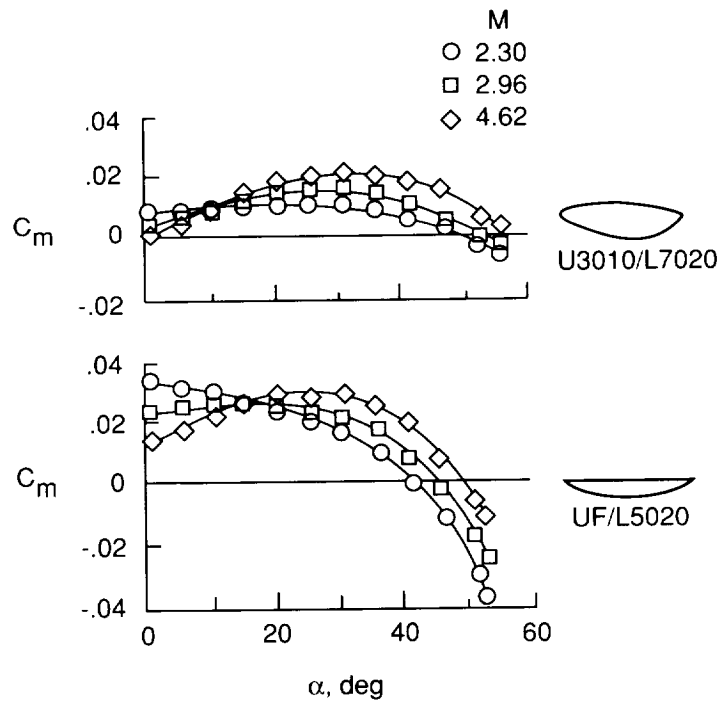


Figure 13. Effect of Mach number on longitudinal characteristics.

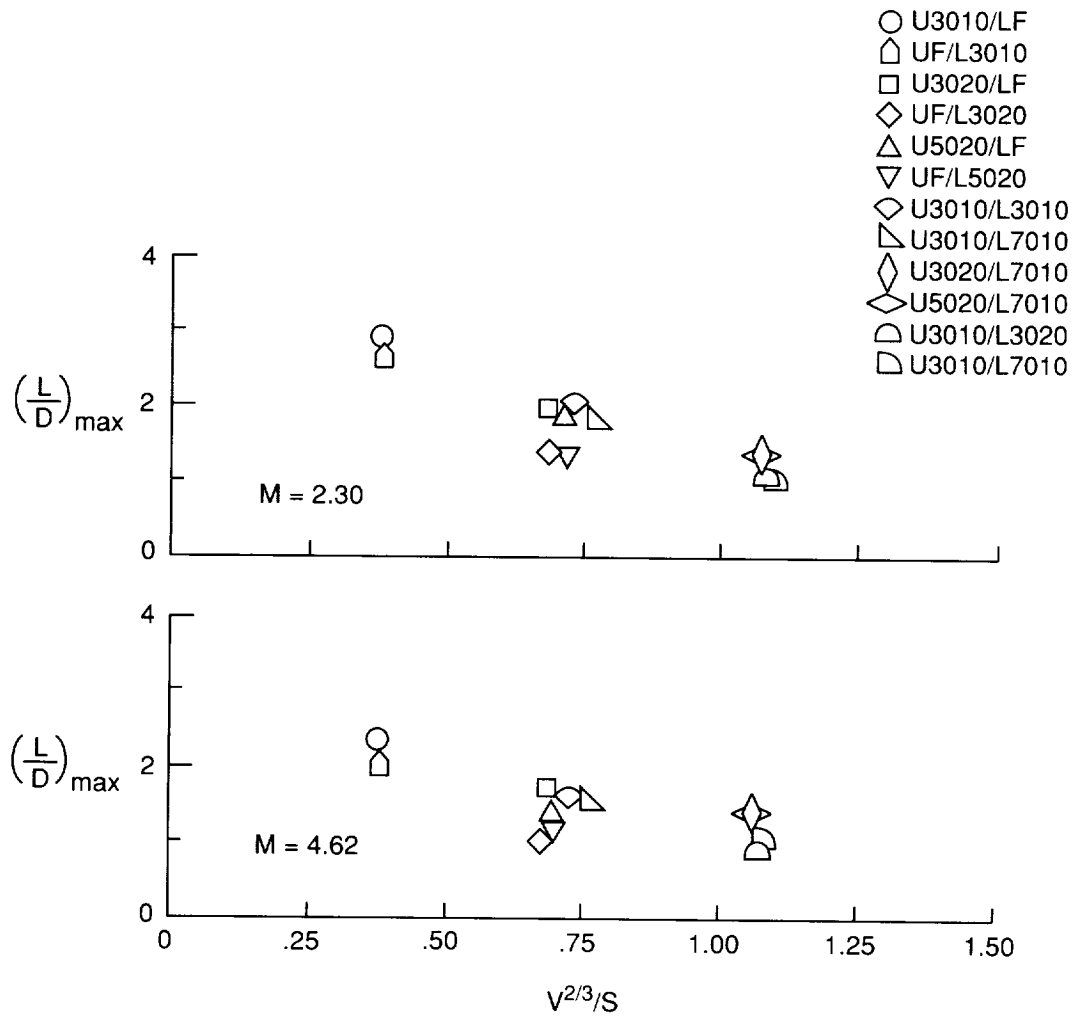


Figure 14. Variation of maximum values of  $L/D$  with volume for each test model at  $M = 2.30$  and  $4.62$ .

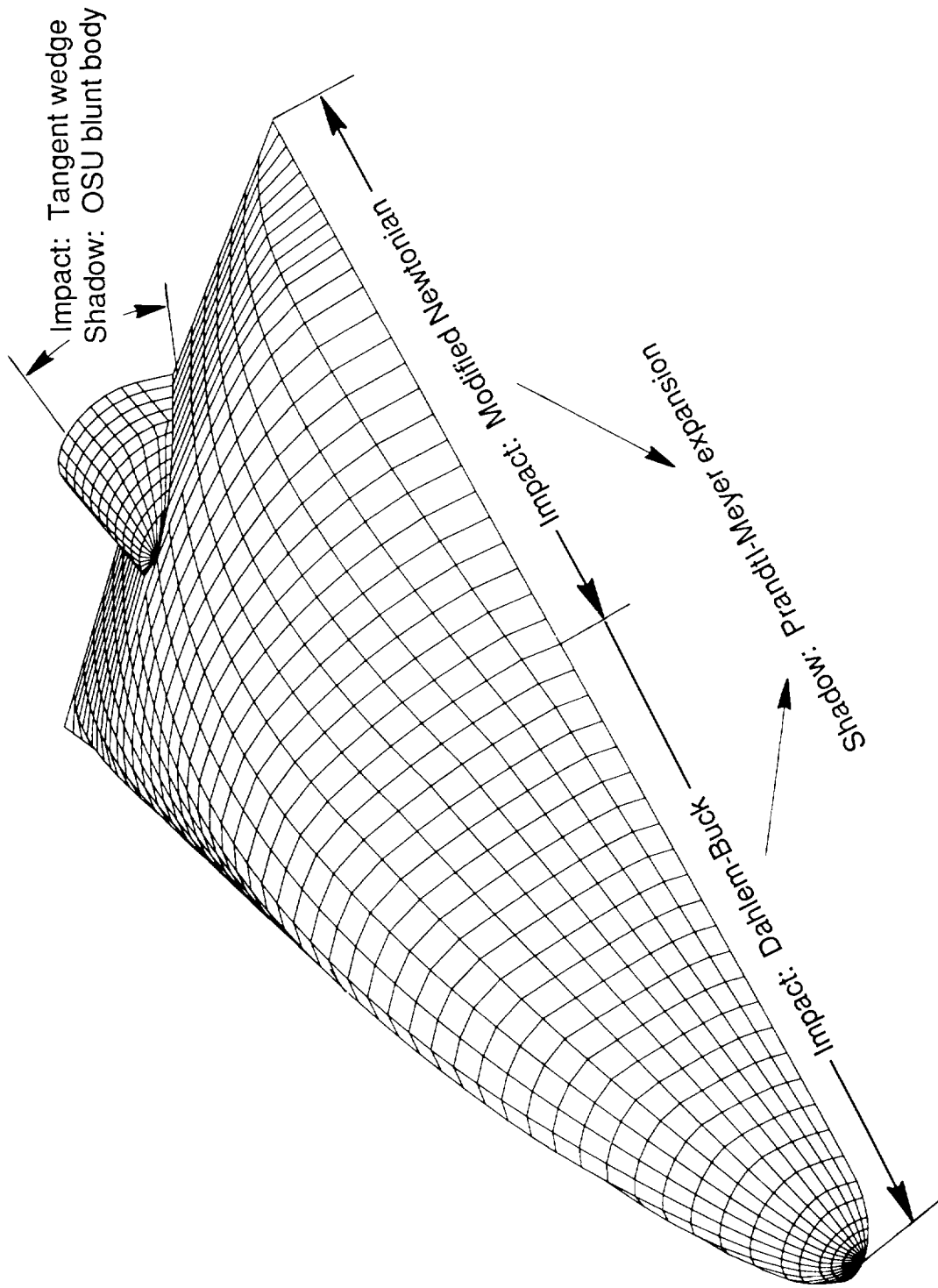


Figure 15. Computer-generated drawing of U5020/LF design illustrating calculative methodology.

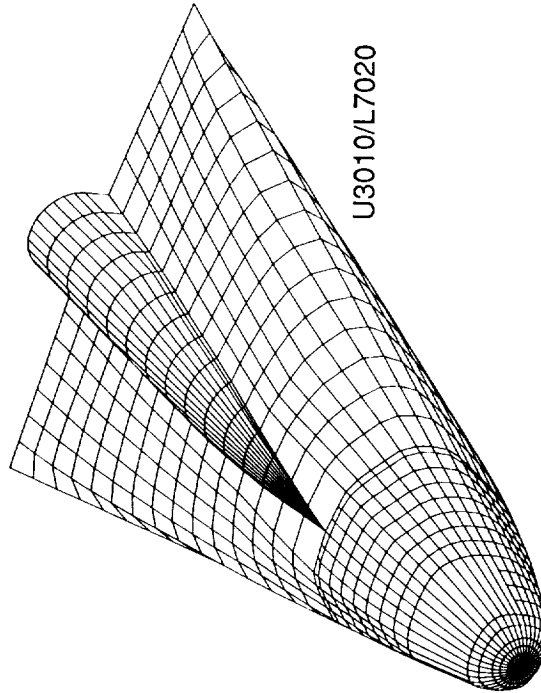
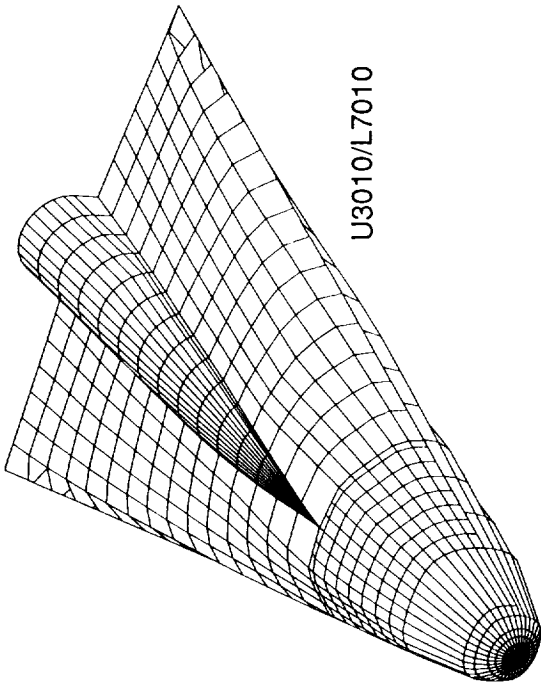
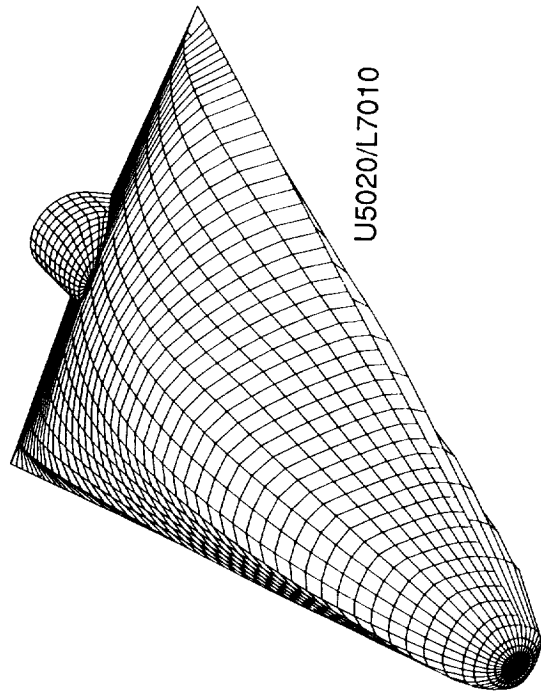
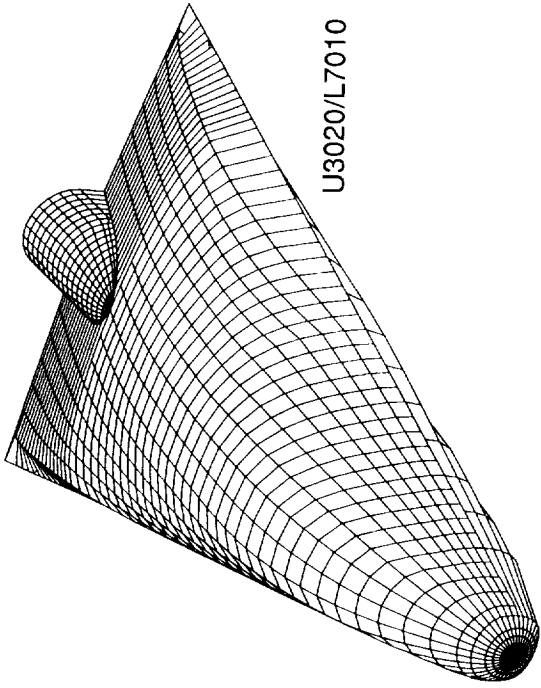


Figure 16. Computer-generated drawings.

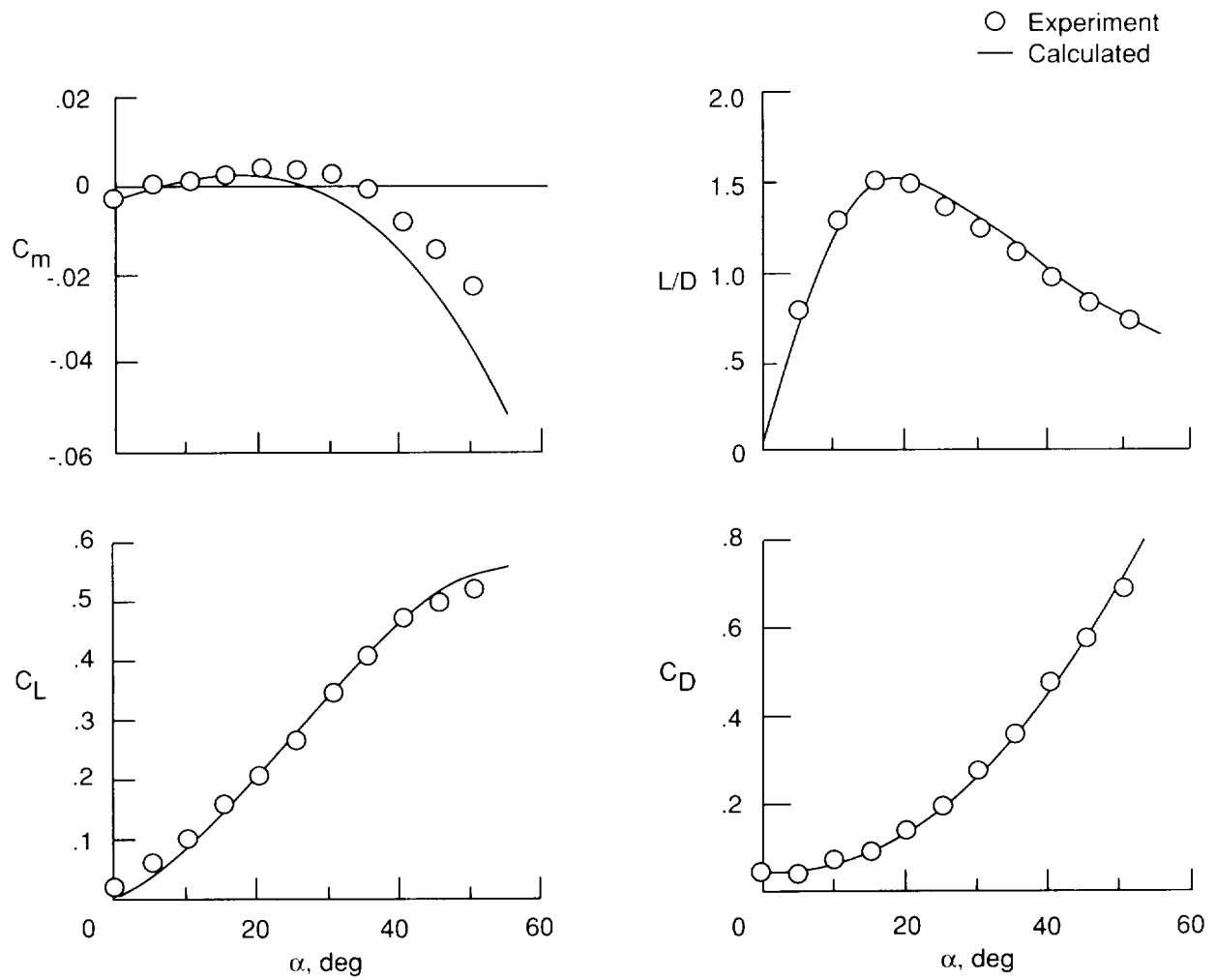


Figure 17. Comparison of calculated and experimental results at  $M = 4.62$  of U3010/L7010.

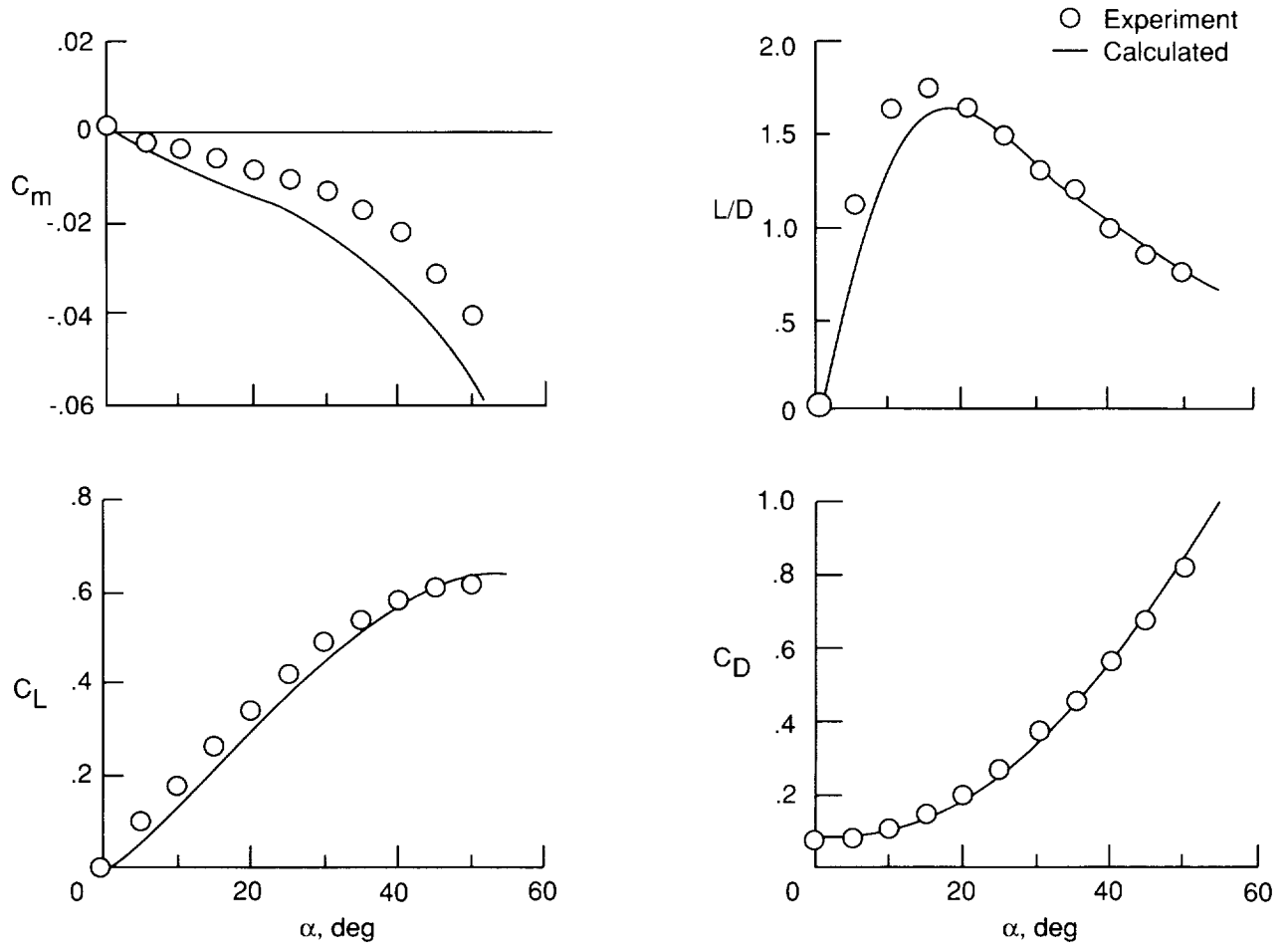


Figure 18. Comparison of calculated and experimental results at  $M = 2.30$  of U3010/L7010.

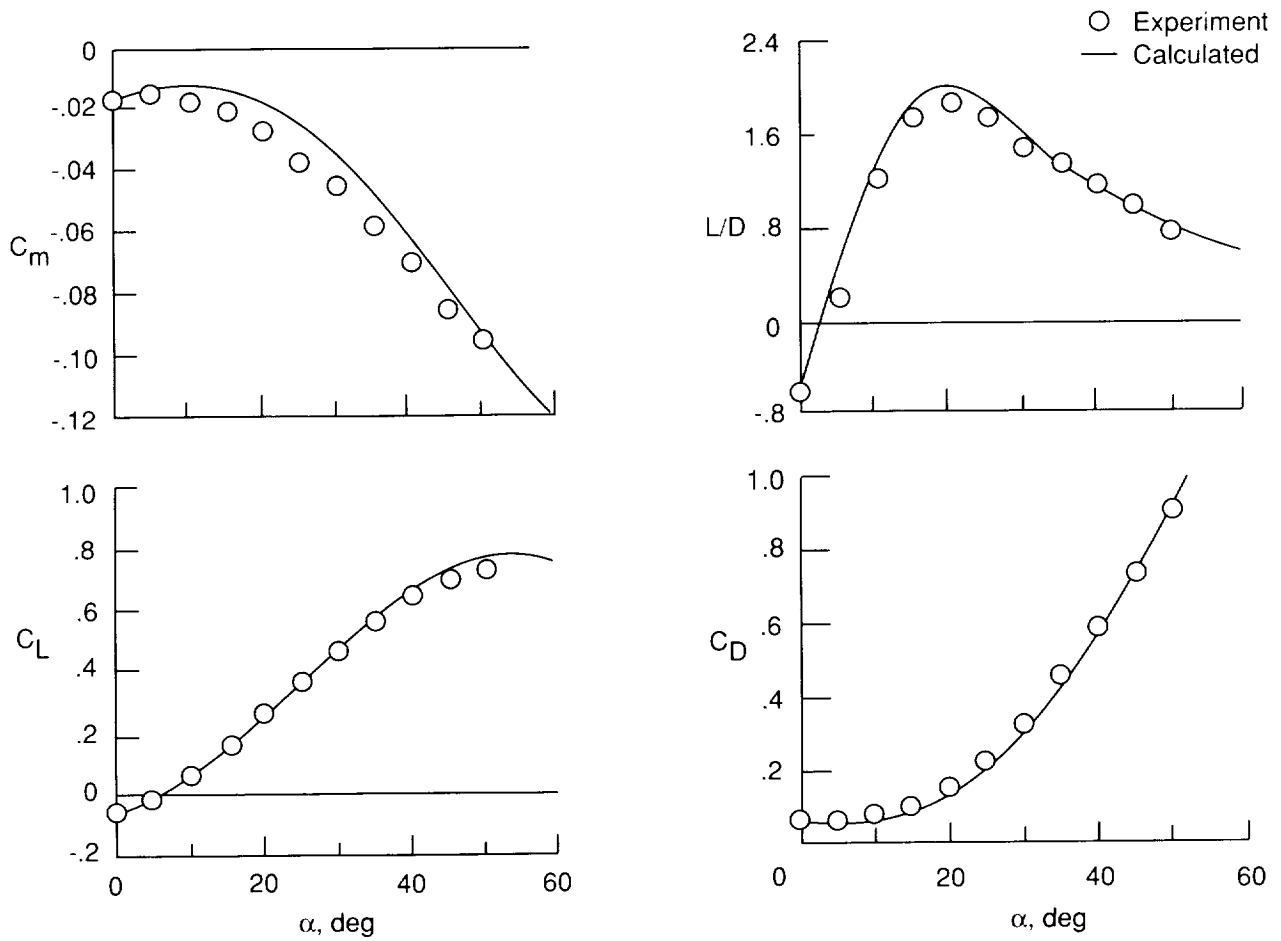
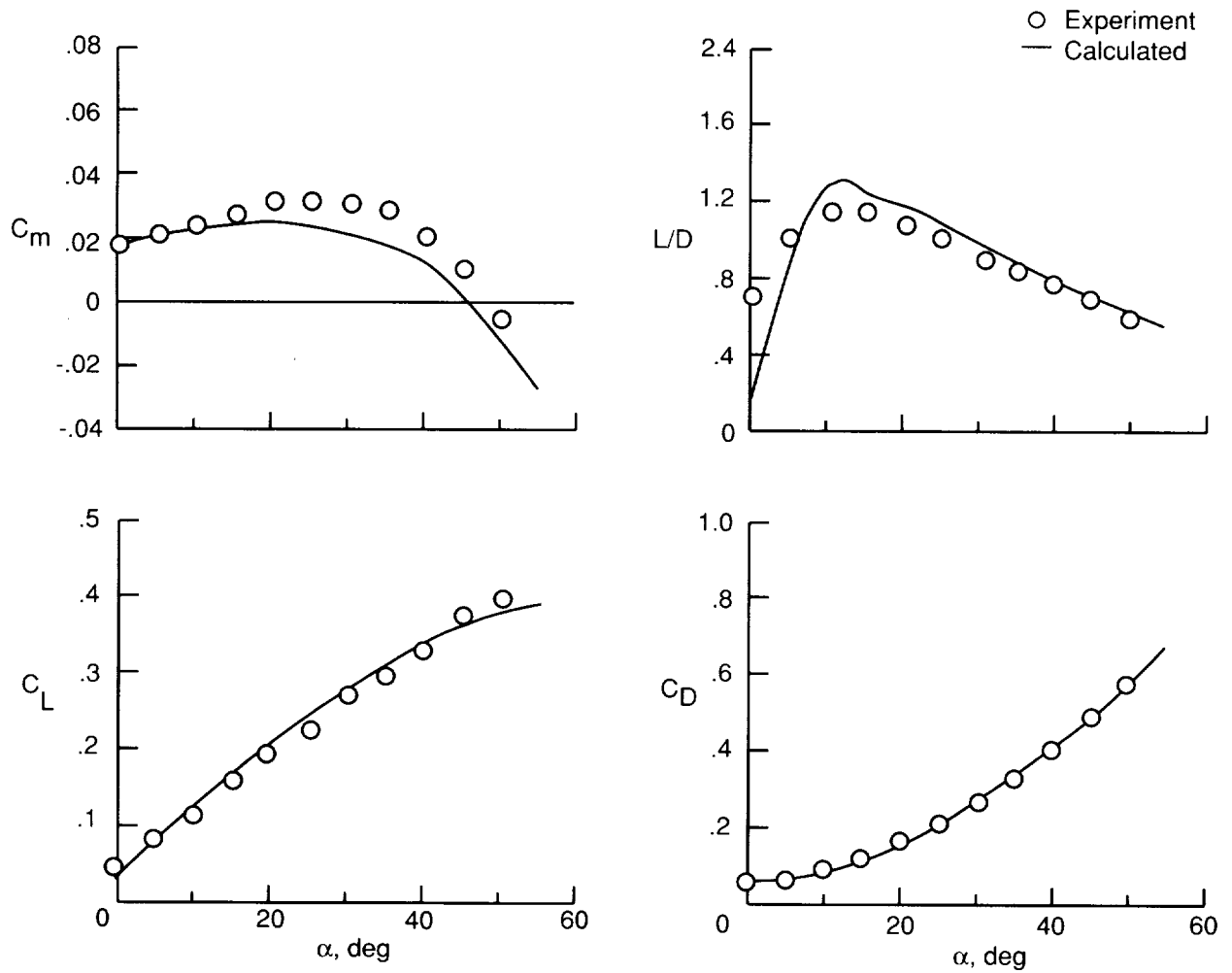
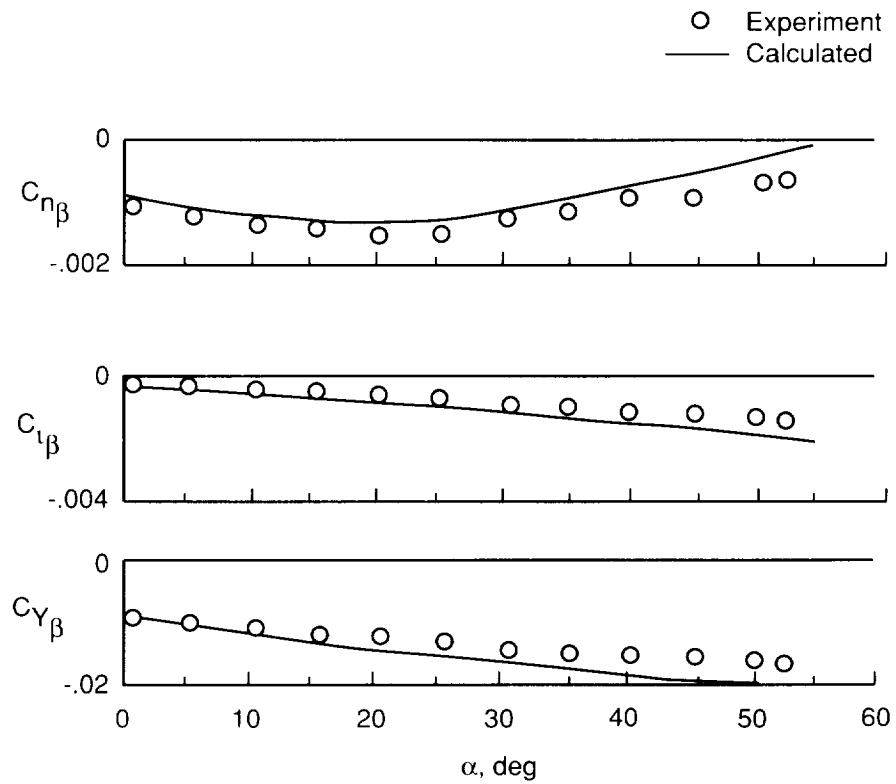


Figure 19. Comparison of calculated and experimental results at  $M = 4.62$  of U5020/LF.



(a) Longitudinal characteristics.

Figure 20. Comparison of calculated and experimental results at  $M = 4.62$  of UF/L5020.



(b) Lateral-directional characteristics.

Figure 20. Concluded.



REPORT DOCUMENTATION PAGE			Form Approved OMB No. 0704-0188	
Public reporting burden for this collection of information is estimated to average 1 hour per response, including the time for reviewing instructions, searching existing data sources, gathering and maintaining the data needed, and completing and reviewing the collection of information. Send comments regarding this burden estimate or any other aspect of this collection of information, including suggestions for reducing this burden, to Washington Headquarters Services, Directorate for Information Operations and Reports, 1215 Jefferson Davis Highway, Suite 1204, Arlington, VA 22202-4302, and to the Office of Management and Budget, Paperwork Reduction Project (0704-0188), Washington, DC 20503				
1. AGENCY USE ONLY (Leave blank)	2. REPORT DATE March 1994	3. REPORT TYPE AND DATES COVERED Technical Memorandum		
4. TITLE AND SUBTITLE Experimental and Theoretical Study of Aerodynamic Characteristics of Some Lifting Bodies at Angles of Attack From $-10^{\circ}$ to $53^{\circ}$ at Mach Numbers From 2.30 to 4.62			5. FUNDING NUMBERS WU 505-69-20-01	
6. AUTHOR(S) M. Leroy Spearman and Abel O. Torres				
7. PERFORMING ORGANIZATION NAME(S) AND ADDRESS(ES) NASA Langley Research Center Hampton, VA 23681-0001			8. PERFORMING ORGANIZATION REPORT NUMBER L-17269	
9. SPONSORING/MONITORING AGENCY NAME(S) AND ADDRESS(ES) National Aeronautics and Space Administration Washington, DC 20546-0001			10. SPONSORING/MONITORING AGENCY REPORT NUMBER NASA TM-4528	
11. SUPPLEMENTARY NOTES				
12a. DISTRIBUTION/AVAILABILITY STATEMENT  Unclassified Unlimited  Subject Category 02			12b. DISTRIBUTION CODE	
13. ABSTRACT (Maximum 200 words) Lifting bodies are of interest for possible use as space transportation vehicles because they have the volume required for significant payloads and the aerodynamic capability to negotiate the transition from high angles of attack to lower angles of attack (for cruise flight) and thus safely reenter the atmosphere and perform conventional horizontal landings. Results are presented for an experimental and theoretical study of the aerodynamic characteristics at supersonic speeds for a series of lifting bodies with $75^{\circ}$ delta planforms, rounded noses, and various upper and lower surface cambers. The camber shapes varied in thickness and in maximum thickness location, and hence in body volume. The experimental results were obtained in the Langley Unitary Plan Wind Tunnel for both the longitudinal and the lateral aerodynamic characteristics. Selected experimental results are compared with calculated results obtained through the use of the Hypersonic Arbitrary-Body Aerodynamic Computer Program.				
14. SUBJECT TERMS Lifting bodies; Space transportation; Space vehicles			15. NUMBER OF PAGES 24	
			16. PRICE CODE A03	
17. SECURITY CLASSIFICATION OF REPORT Unclassified	18. SECURITY CLASSIFICATION OF THIS PAGE Unclassified	19. SECURITY CLASSIFICATION OF ABSTRACT	20. LIMITATION OF ABSTRACT	

